Reprinted from Journal of Electroanalytical Chemistry 483 (2000), pp. 37-46

www.elsevier.nl/locate/jelechem

ELSEVIER

Journal of Electroanalytical Chemistry 483 (2000) 37–46

Journal of Electroanalytical Chemistry

Channel flow at an immobilised liquid | liquid interface☆

Peter Liljeroth [a], Christoffer Johans [a], Kyösti Kontturi [a], José A. Manzanares [b,*]

[a] *Laboratory of Physical Chemistry and Electrochemistry, Helsinki University of Technology, PO Box 6100, FIN-02015 Hut, Finland*
[b] *Departament de Termodinàmica, Facultat de Fisica, Universitat de València, E-46100 Burjassot, Spain*

Received 11 August 1999; received in revised form 6 December 1999; accepted 14 January 2000

Abstract

A novel rectangular channel flow electrochemical cell for the study of liquid | liquid interfaces is presented. The organic phase is immobilised by the use of a gelling agent, while the aqueous phase flows past the interface. This creates an asymmetric setup that allows us to establish diagnostic criteria to determine, for example, the direction of the ion transfer. The effects of varying flow rate and sweep rate have been considered both theoretically and experimentally. By comparison with two-dimensional simulations, it is demonstrated that a simple one-dimensional theory can be used to describe the cyclic voltammetry response of the channel flow cell. © 2000 Elsevier Science S.A. All rights reserved.

Keywords: ITIES; Ion transfer; Hydrodynamic methods; Channel flow; Immobilised interfaces

1. Introduction

Traditionally, theories and techniques used for the study of ion transfer across the interface between two immiscible electrolyte solutions (ITIES) have been transposed directly from those existing for the electrode | solution interface. This is particularly true for systems with well-defined hydrodynamics, which so far include micropipettes [1], microholes [2], dropping electrolyte electrodes [3], wall-jet configurations with an immobilised organic phase [4,5], thin-layer flow-through cells [6], and rotating diffusion cells [7]. Ion transfer across ITIES involves mass transport across two diffusion boundary layers and an interfacial transfer step. The main difficulty in the study of these processes arises from the fact that the interfacial kinetics are typically fast, with standard rate constants $k^0 > 0.1$ cm s^{-1}. The reason why the systems with enhanced mass transfer have received so much attention is that any attempt to extract kinetic information requires an accurate control over the rate of mass transport. In practice, however, the ion transfer across ITIES is so fast that it is difficult to obtain kinetic parameters even in these systems with enhanced mass transfer. Nevertheless, systems with well-defined hydrodynamics are worth considering for other reasons. On the one hand, the electrochemical response of ITIES in techniques such as cyclic voltammetry can often be modelled by assuming reversible ion transfer, and the description of the mass transport process there involved is more accurate in systems with known hydrodynamics. On the other hand, the asymmetry of the diffusion fields at, for instance, ITIES supported at the tip of a micropipette, provides diagnostic criteria concerning the direction of ion transfer and insight into the mechanism of more complex charge transfer reactions.

In this work, we report on the feasibility of using a rectangular channel flow cell (CFC) for the study of ion transfer processes at immobilised liquid | liquid interfaces. The experiments carried out aim at presenting the basic trends of this novel system in relation to the effects of varying the flow rate of the aqueous phase and the sweep rate. In addition, the asymmetry of the diffusion fields (linear diffusion in the organic phase and convective diffusion in the aqueous phase) allows the determination of the direction of ion transfer. We aim also at providing a simple theoretical background for analysing the experimental results and discussing some of the distinctive features of this system.

☆ Paper presented at the Euroconference on Modern Trends in Electrochemistry of Molecular Interfaces, Finland, 28 August–3 September, 1999.

* Corresponding author. Fax: +34-96-3983385.
E-mail address: manzanar@uv.es (J.A. Manzanares)

0022-0728/00/$ - see front matter
PII: S0022-0728(00)00029-2

In relation to the theoretical modelling and simulations, we have benefited from a vast amount of work carried out previously for charge transfer processes at electrode | solution interfaces in tubular and rectangular CFCs. Following this work, we have aimed at showing that the one-dimensional simulations making use of the Singh and Dutt approximation yield, e.g. cyclic voltammograms, which closely resemble those obtained from more accurate two-dimensional simulations. In doing so, we prove the validity of the Singh and Dutt approximation for liquid | liquid systems, and justify the future use of these much simpler one-dimensional models for the analysis of experimental data on, e.g. facilitated ion transfer and electron transfer coupled with homogeneous chemical reactions. However, other applications such as mechanistic studies taking advantage of the non-uniform accessibility of the channel flow ITIES [8–10] or using detector interfaces [11], might require two-dimensional simulations.

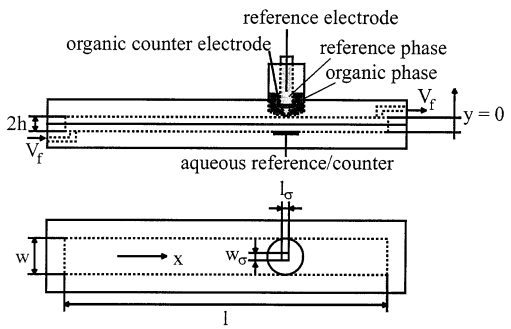

Fig. 1. Schematic presentation of the channel flow cell employed.

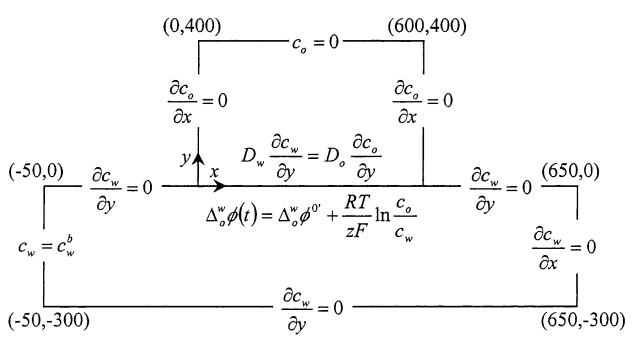

Fig. 2. Schematic presentation of the boundary conditions used. The organic phase is depicted on top of the aqueous phase. The magnitudes involved in the condition of reversible ion transfer are: $\Delta_o^w\phi^{0'}$ formal standard transfer potential, z charge number, F Faraday's constant, R gas constant, and T absolute temperature. The coordinates refer to values of (X, Y).

2. Theory

2.1. Two-dimensional formulation

The ITIES under study is oriented horizontally (see Fig. 1) and is defined by Cartesian coordinates $y = 0$, $0 \le x \le l_\sigma$, $0 \le z \le w_\sigma$. The immobilised organic phase is located in the region $y > 0$ and the flowing aqueous phase in the region $-2h < y < 0$, where $2h$ is the channel height. The flow direction is along the positive x-axis, and the width w of the channel along the z-direction is assumed to be so large that the transport can be described as two-dimensional.

Since both solutions contain supporting electrolyte, migration is neglected and the convective-diffusion equations of the transferring ion take the form

$$\frac{\partial c_w}{\partial t} = D_w\left(\frac{\partial^2 c_w}{\partial x^2} + \frac{\partial^2 c_w}{\partial y^2}\right) - v_x\frac{\partial c_w}{\partial x} \tag{1a}$$

$$\frac{\partial c_o}{\partial t} = D_o\left(\frac{\partial^2 c_o}{\partial x^2} + \frac{\partial^2 c_o}{\partial y^2}\right) \tag{1b}$$

Fully-developed Poiseuille flow is assumed

$$v_x = v_m\left[1 - \frac{(h+y)^2}{h^2}\right] \qquad -2h \le y \le 0 \tag{2}$$

where v_m is the maximum flow velocity (at the channel centre). Within ca. 10% error (for the cell used in this work) due to the effect of finite w, the velocity v_m is related to the volume flow rate V_f by $V_f \approx (4/3)hwv_m$ [12].

For the sake of simplicity, only the case when the transferring ion is initially present in the aqueous phase is considered, and therefore the initial conditions are

$$c_w(x, y, t = 0) = c_w^b \quad -\infty < x < \infty \quad -2h \le y \le 0 \tag{3a}$$

$$c_o(x, y, t = 0) = 0 \quad 0 \le x \le l_\sigma \quad 0 \le y < \infty \tag{3b}$$

The boundary conditions are presented schematically in Fig. 2. The condition of reversible ion transfer is imposed with the same value $\Delta_o^w\phi(t)$ at every point along the interface because in the presence of supporting electrolyte the electrical potential gradients are negligible. In the case of cyclic voltammetry the potential difference $\Delta_o^w\phi(t)$ is given by

$$\Delta_o^w\phi(t) = \Delta_o^w\phi_i + v(t_\lambda - |t_\lambda - t|) \quad 0 \le t \le 2t_\lambda \tag{4}$$

where v is the sweep rate, t_λ is the switching time, and $\Delta_o^w\phi_i$ is the initial potential difference.

These transport equations can be solved numerically (see Appendix A for details) and then the current can be calculated by integration over the interface

$$I(t) = -zFD_w w_\sigma \int_0^{l_\sigma} \left.\frac{\partial c_w}{\partial y}\right|_{y=0} dx \tag{5}$$

2.2. One-dimensional formulation

The transport problem can be formulated as one-dimensional by introducing the average concentrations $\overline{c_w}$ and $\overline{c_o}$ over the interface length, $0 \le x \le l_\sigma$, and neglecting axial diffusion [13,14]. Considering that the concentration at the edges of the interface can be approximated by c_w^b (upstream) and $\overline{c_w}$ (downstream), the spatial averages of Eqs. (1a) and (1b) over the interface length are

$$\frac{\partial \overline{c_w}}{\partial t} = D_w \frac{\partial^2 \overline{c_w}}{\partial y^2} - v_x \frac{\overline{c_w} - c_w^b}{l_\sigma} \tag{6a}$$

$$\frac{\partial \overline{c_o}}{\partial t} = D_o \frac{\partial^2 \overline{c_o}}{<RO> \partial y^2} \tag{6b}$$

This method of solution is called the Singh and Dutt approximation [15,16]. The boundary conditions for Eqs. (6a) and (6b) are

$$\lim_{y \to -\infty} \overline{c_w} = c_w^b \tag{7a}$$

$$\lim_{y \to \infty} \overline{c_o} = 0 \tag{7b}$$

$$D_w \frac{\partial \overline{c_w}}{\partial y} = D_o \frac{\partial \overline{c_o}}{\partial y} \qquad y = 0 \tag{8}$$

$$\Delta_o^w \phi(t) = \Delta_o^w \phi^{o'} + \frac{RT}{zF} \ln \frac{\overline{c_o}}{\overline{c_w}} \qquad y = 0 \tag{9}$$

where Eqs. (7a) and (7b) assume that extension of the solutions along the y-axis is much larger than the diffusion layer. In agreement with the assumption involved in Eq. (7a), the flow velocity is approximated by

$$v_x \approx -2 v_m \frac{y}{h} \tag{10}$$

which is known as Lévêque's approximation [17]. From the numerical solution of these one-dimensional transport equations (see Appendix B for details), the current can be calculated as

$$I(t) = -z F D_w w_\sigma l \sigma \left. \frac{\partial \overline{c_w}}{\partial y} \right|_{y=0} \tag{11}$$

The limiting current, however, can be easily obtained analytically. Because $\overline{c_w}$ is independent of time under limiting conditions, Eq. (6a) can be reduced to Airy's equation [18]. The solution of this equation is

$$\overline{c_w} = c_w^b \left[1 - \frac{\mathrm{Ai}(\xi)}{\mathrm{Ai}(0)} \right] \tag{12}$$

where $\xi \equiv -Pe^{1/3}(y/h)$ and Ai is Airy's function. The Peclet number $Pe \equiv 3V_f h/(2D_w w l_\sigma)$ represents the magnitude of the convective flow with respect to the diffusive flow and is equal to twice the ratio of the time $t_{diff} = h^2/D_w$ required to diffuse across a distance h and the time $t_{conv} = l_\sigma / v_m$ required to travel by convection along the interface length l_σ. Substituting Eq. (12) into Eq. (11) leads then to the limiting current

$$I_L = -z F D_w w_\sigma l_\sigma Pe^{1/3} \frac{c_w^b}{h} \frac{\mathrm{Ai}'(0)}{\mathrm{Ai}(0)}$$

$$= 0.835\, zF w_\sigma c_w^b \left(\frac{l_\sigma^2 D_w^2 V_f}{h^2 w} \right)^{1/3} \tag{13}$$

A similar equation was derived by Levich [13] from the solution of Eqs. (1a) and (10) and neglecting the axial diffusion, which yielded a numerical coefficient of 0.925 instead of 0.835. This difference is due to the Singh and Dutt approximation [15].

2.3. Dimensionless sweep rate

The electrochemical response of the CFC is ruled by the time dependence of the applied potential difference $\Delta_o^w \phi(t)$ and the time dependence of the concentration changes due to the convective-diffusion process. Thus, in order to determine whether a sweep rate is fast or slow, it must be compared with the characteristic times involved in the process. Since convective diffusion involves two characteristic times, t_{diff} and t_{conv}, the time evolution of concentration is determined by a combination of t_{diff} and t_{conv}. Such a combination can be found out from Eqs. (6a), (11) and (12). Indeed, Eq. (12) shows that the diffusion and convection terms in Eq. (6a) are of the same order when the changes in y are of the order of $Pe^{-1/3}h$. Hence, it was deduced from Eq. (6a) that the changes in concentration with time are of the same order as those associated with either diffusion or convection after a characteristic time $t_{diff} Pe^{-2/3} \sim t_{conv} Pe^{1/3} \sim t_{diff}^{1/3} t_{conv}^{2/3}$. Therefore, it was concluded that the shape of the voltammogram is uniquely determined by the dimensionless sweep rate [19]

$$\sigma = \frac{z F v}{RT} t_{diff} Pe^{-2/3} = \frac{z F v}{RT} \left(\frac{2h^2 l_\sigma w}{3 V_f D_w^{1/2}} \right)^{2/3} \tag{14}$$

provided that the initial potential $\Delta_o^w \phi_i$ is such that no faradaic current is flowing.

3. Experimental

The cell used is shown in Scheme 1.

The organic solvent was 2-nitrophenyl octyl ether (NPOE, Fluka, Selectophore®). The organic supporting electrolyte was tetraphenylarsonium tetrakis-4-(chloro)phenylborate ($TPAsTPBCl_4$), prepared by metathesis of tetraphenylarsonium chloride (TPAsCl,

Ag	AgCl	5 mM $TPAsCl_4$ (aq)	10 mM $TPAsTPBCl_4$ 10 w-% PVC (NPOE)	100 mM LiCl 0.4 mM TEACl (aq)	AgCl	Ag

Scheme 1.

Sigma, p.a.) and potassium tetrakis-4-chlorophenylborate ($KTPBCl_4$, Aldrich, p.a.) as described elsewhere [20]. The organic phase was immobilised by polyvinylchloride (PVC, Sigma, very high molar mass) [21]. The aqueous supporting electrolyte was lithium chloride (LiCl, Riedel-de Haen, p.a.) and the transferring ion was tetraethylammonium ion (TEA^+), which was added to the aqueous phase as a chloride salt (TEACl, Sigma, p.a.). All the aqueous solutions were prepared from Milli-Q® water.

A schematic drawing of the CFC is presented in Fig. 1. The dimensions of the cell are as follows: length $l = 135$ mm, width $w = 15.3$ mm, half-height of the channel $h = 1.0$ mm, and interface length and width $l_\sigma = w_\sigma = 3.0$ mm. The cell was made of Delrin (Du Pont, Inc.). A 4-electrode potentiostat (Southampton University, UK) with positive feedback *IR* compensation was run in 3-electrode mode by short-circuiting the aqueous reference and counter terminals. The potential was controlled by a waveform generator PPR1 (Hi-Tek Instruments, UK) and the resulting current was measured with a Tektronix TDS420A four channel digitizing oscilloscope (Tektronix Inc. USA). The flow rate of the aqueous phase was controlled by a peristaltic pump (Ismatec IPN-12, Switzerland) and typically varied between 100 and 1000 $cm^3\ h^{-1}$. The peristaltic pulse was eliminated by the use of a damping system consisting of a T-shaped air filled tubing, followed by a high flow resistance.

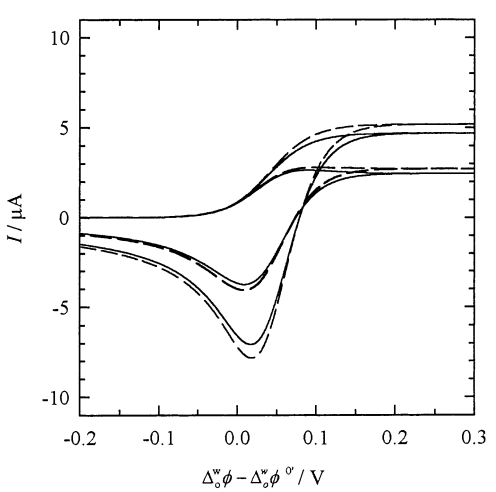

Fig. 3. Comparison between the Singh and Dutt approximation (solid line) and the solution to the full, two-dimensional problem (dashed line). Sweep rate 5 mV s^{-1}. Flow rates 100 and 700 $cm^3\ h^{-1}$. Other parameter values: $D_w = 1 \times 10^{-5}$ $cm^2\ s^{-1}$, $D_o = 5 \times 10^{-7}$ $cm^2\ s^{-1}$, and $c_w^b = 0.1$ mM. The dimensions of the channel and the interface are the same as in the experimental part: $h = 1.0$ mm, $w = 15.3$ mm, $l_\sigma = 3.0$ mm, $w_\sigma = 3.0$ mm.

4. Results

4.1. Simulations

The transport problems considered in this paper cannot be solved analytically. Thus, numerical methods have to be used. The one-dimensional problem was solved by an explicit finite difference method. The alternating direction implicit (ADI) method was used for the two-dimensional diffusion problem. Details of procedures are given in the Appendices.

The validity of the Singh and Dutt approximation at a liquid | liquid channel flow was assessed by comparing the solution with that of the full two-dimensional diffusion problem. Comparison between typical results from the one- and two-dimensional models is shown in Fig. 3. The comparison was equally favourable over a range of flow and sweep rates. The correspondence would be even better if the currents were scaled by the limiting current. The validity of the Singh and Dutt approximation has been thoroughly tested at metal electrodes [16,22], and it seems that applying it to a liquid | liquid interface does not break the validity of the assumption. The quality of the results based on the Singh and Dutt approximation is further manifested in the dependence of the half-wave potential on the dimensionless sweep rate that will be discussed later.

Concentration profiles obtained from the two-dimensional simulation at the limiting current in a cyclic voltammetry simulation are displayed in Fig. 4(a) and (b). The x and y-axis have been rendered dimensionless by scaling to the interface length l_σ and the channel height $2h$, respectively. It should be noted that the difference in the actual lengths of the axis is roughly a factor of ten. Thus, the concentration gradient normal to the interface is much steeper than the gradient along the axial direction. Because the thickness of the diffusion boundary layer is observed to be much smaller than the channel height, it is evident that the cell does not behave as a thin layer cell, i.e. there is no exhaustive electrolysis through the whole channel cross section. Thus, the boundary condition (Eq. (7a)) is justified. At the outer edge of the diffusion boundary layer ($y/2h \approx 0.15$), the linearised velocity profile differs from the parabolic one by 17%. However, the velocity enters the transport equations only multiplied by the axial concentration gradient, which is very small for the outer half of the diffusion boundary layer. Thus the error in the calculated current is much less than the difference in the actual velocities. In fact, it was found to be within 1% for the experimental range of sweep and flow rates. This observation is in agreement with the fact that the criterion $Pe \gg 1$ for the validity of the linearisation given by Compton and Coles [23] is fulfilled with the present setup. It is difficult to give graphical arguments based on Fig. 4 to support the validity

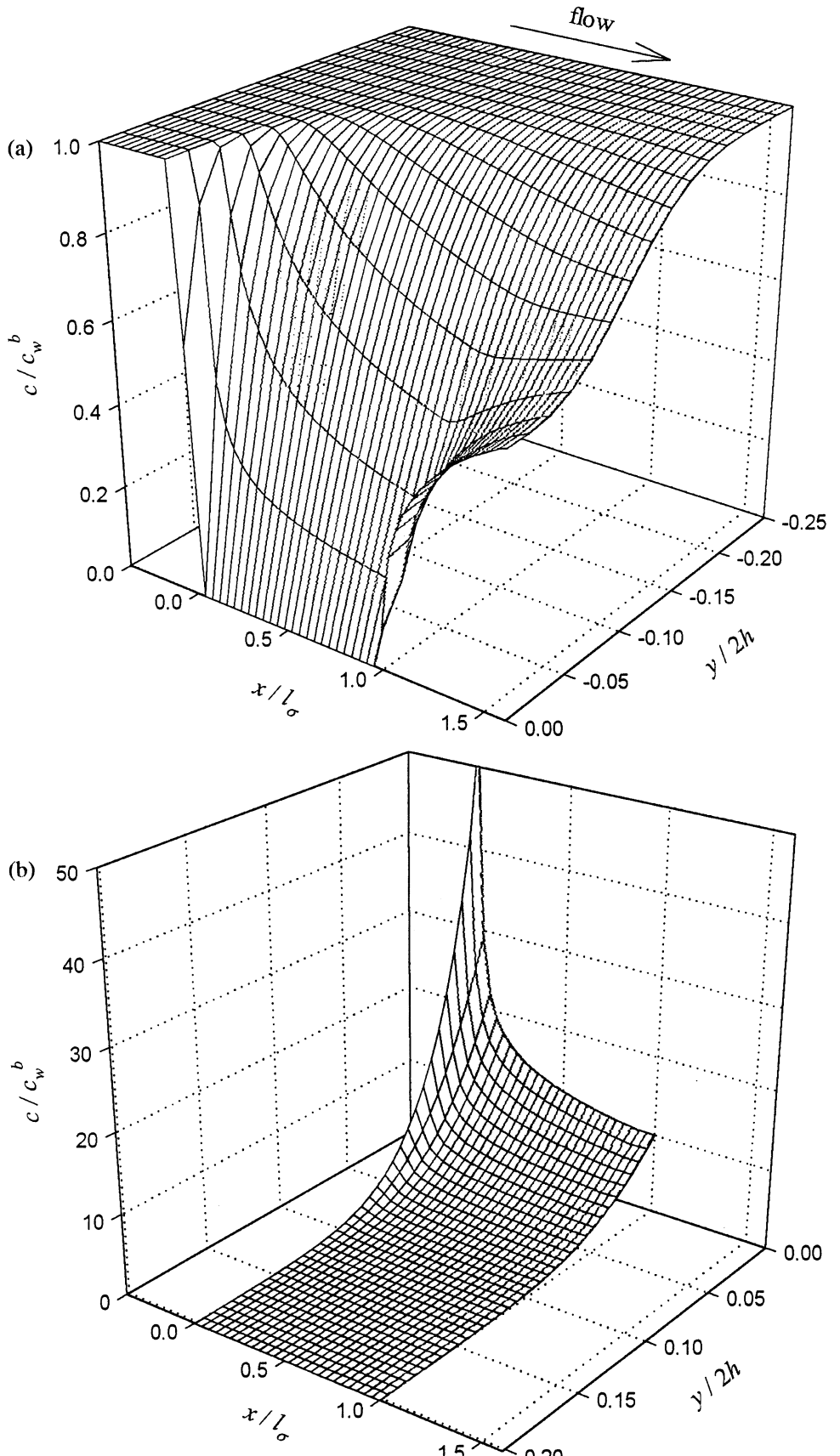

Fig. 4. Simulated concentration profiles from the two-dimensional model at the limiting current in the aqueous (a) and in the organic (b) phase. Flow rate 100 $cm^3\ h^{-1}$. Sweep rate 2 $mV\ s^{-1}$. Other parameter values as in Fig. 3.

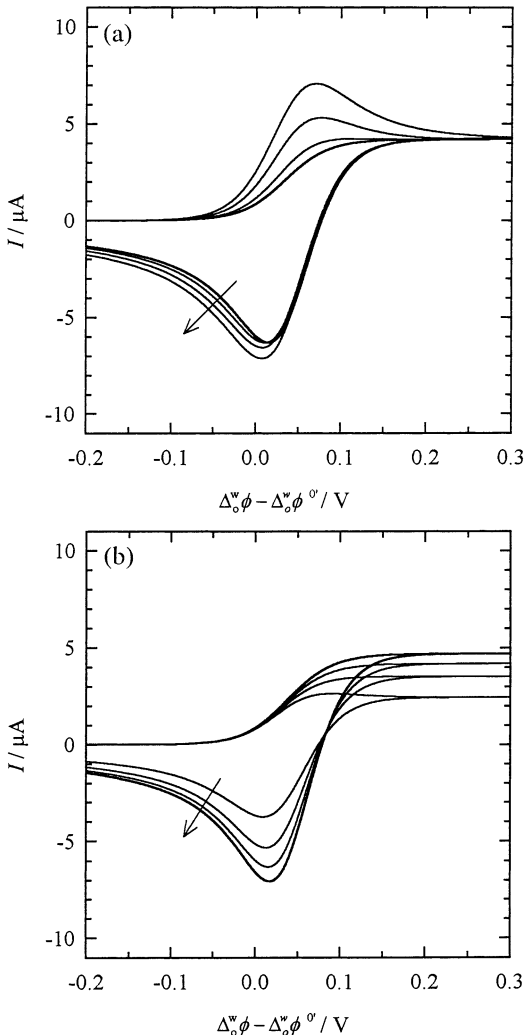

Fig. 5. (a) The sweep rate dependence of the simulated voltammograms of ion transfer from the aqueous to the organic phase. Flow rate 500 $cm^3\ h^{-1}$. Sweep rates 5, 10, 25, and 50 mV s^{-1}. Other parameter values as in Fig. 3. The arrow shows the direction of increasing v. (b) The effect of the flow rate on the simulated voltammograms of ion transfer from the aqueous to the organic phase. Sweep rate 5 mV s^{-1}. Flow rates 100, 300, 500, and 700 $cm^3\ h^{-1}$. Other parameter values as in Fig. 3. The arrow shows the direction of increasing V_f.

of the Singh and Dutt approximation. However, Fig. 3 has shown that it works very well over a range of sweep and flow rates. The same surprising quantitative agreement between the Singh and Dutt approximation and more rigorous two-dimensional models has also been noted at metal electrodes [16,22]. One remarkable feature of the concentration profile in the organic phase (Fig. 4(b)) is the fairly high interfacial concentration. This was observed on all the simulations, not just that shown in Fig. 4(b). It is due to the low value of the diffusion coefficient in the organic phase and the continuity of flux across the interface.

As was noted, the agreement between the Singh and Dutt approximation and the more elaborate solution is rather good. Given the quality and accuracy of the results obtained from the Singh and Dutt approximation and its simplicity, the simulated voltammograms shown in Fig. 5(a) and (b) have been calculated under this approximation. The effect of sweep rate is considered in Fig. 5(a). As the sweep rate is decreased, the forward scan evolves from a peak-shaped response to a steady-state-like wave. This is due to the interplay between diffusion and convection: at higher sweep rates (shorter time scales) linear diffusion is comparable to the convective component of the mass transport and at lower sweep rates (longer time scales) the convective component dominates the mass transport in the aqueous phase. However, due to the linear diffusion in the immobilised organic phase, in the absence of natural convection effects, the current will not approach steady state as the sweep rate is lowered. This point will be elaborated in more detail later. The effect of the flow rate is considered in Fig. 5(b) and it can be seen that the limiting current increases with increasing flow rate. Also, the voltammograms in Fig. 5(a) and (b) suggest that there is only one independent parameter that determines the shape of the current response (see Eq. (14)). Note, for instance, that decreasing the flow rate from 500 to 100 $cm^3\ h^{-1}$ in Fig. 5(b) has a similar effect on the shape of the voltammogram as increasing the sweep rate from 5 to 25 mV s^{-1} in Fig. 5(a).

4.2. Experimental results

The base electrolyte voltammograms are presented in Fig. 6. Due to the asymmetric diffusion regime, the species limiting the size of the available potential window can be inferred. On the reverse scan, ion transfer from the immobilised phase yields a peak-shaped response, whereas the transfer from the flowing phase by convective diffusion gives rise to a steady state wave-

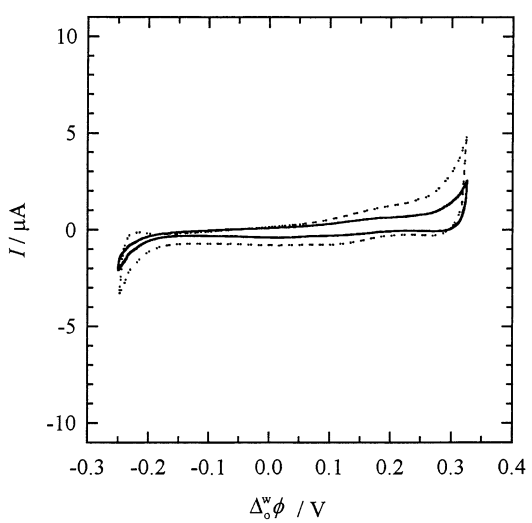

Fig. 6. Experimental base electrolyte voltammograms at the channel flow water | immobilised o-NPOE interface. Flow rate 520 $cm^3\ h^{-1}$. Sweep rates 2 mV s^{-1} (solid line) and 10 mV s^{-1} (dashed line).

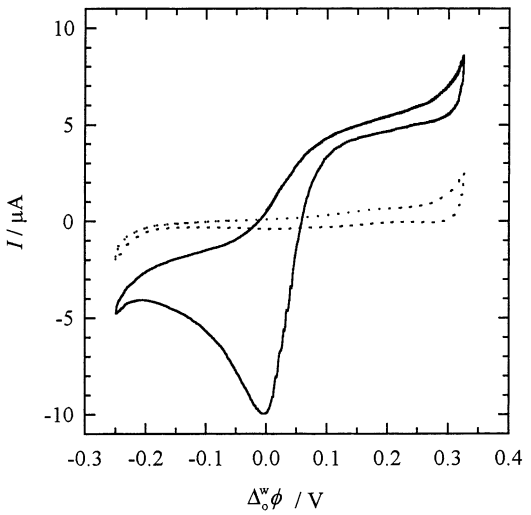

Fig. 7. Experimental cyclic voltammograms of TEA^+ transfer (solid line) and base electrolyte (dashed line) at the channel flow water | immobilised *o*-NPOE interface. Flow rate 525 $cm^3\ h^{-1}$. Sweep rate 2 mV s^{-1}.

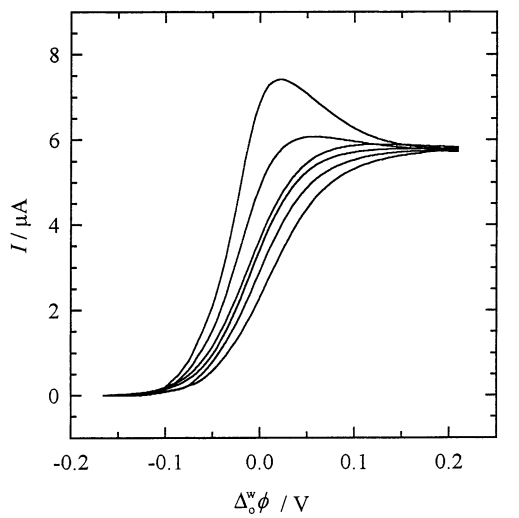

Fig. 8. Effect of the varying sweep rate on the experimental linear potential sweeps of TEA^+ transfer across the channel flow water | immobilised *o*-NPOE interface. Flow rate 520 $cm^3\ h^{-1}$. Sweep rates 2, 5, 8, 10, 15, and 25 mV s^{-1}.

shaped voltammogram at low enough sweep rates. Thus, from the shape of the edge of the window, it can be deduced that the aqueous cation (Li^+) and the organic cation ($TPAs^+$) limit the positive and the negative edges of the window, respectively. The non-zero current in the positive part of the potential windows is most likely due to an impurity in the organic base electrolyte. Fig. 7 shows the voltammogram in the presence of a probe ion (TEA^+). The asymmetric shape is clearly seen, the rate of ion transfer from the aqueous to the organic phase is controlled by convective diffusion, hence resulting in a pseudo-steady-state wave. On the other hand, the transfer from the organic to the aqueous phase is controlled by the rate of linear diffusion, resulting in a peak-shaped voltammogram.

If the forward scan of a cation transfer from the aqueous to the organic phase is considered, the shape of the voltammogram is expected to evolve from wave-like to peak-shaped as the sweep rate is increased. This is experimentally verified, as shown in Fig. 8. It must be borne in mind that there is no true steady state as the sweep rate is decreased; the current tends to zero as the sweep rate approaches zero, due to the linear diffusion in the organic phase. In the absence of natural convection effects there is no steady-state solution for the linear diffusion apart from the trivial one. Similar conclusions about the apparent steady state at a micropipette-supported interface have been reached by Ohkouchi et al. [24].

Linear sweep voltammograms at different volumetric flow rates are shown in Fig. 9. The half-wave potential is not a constant. This is due to changing the dimensionless sweep rate, which in reality determines the half-wave potential. The diffusion coefficient of the transferring ion can be determined by plotting the limiting current as a function of the cubic root of the flow rate (Fig. 10). From the slope of the linear fit, a value of $(1.2 \pm 0.2) \times 10^{-5}$ $cm^2\ s^{-1}$ for the diffusion coefficient of TEA^+ was obtained. This value compares favourably with the value of 1.0×10^{-5} $cm^2\ s^{-1}$ obtained from standard four-electrode cyclic voltammetry.

The difference between the half-wave potential $\Delta_o^w\phi_{1/2}$, i.e. the potential at which the current is half of the limiting value, and the reversible half-wave potential [25], $\Delta_o^w\phi_{1/2,rev}$ as a function of the dimensionless sweep rate, Eq. (14), is plotted in Fig. 11. The reversible half-wave potential contains a term $(RT/zF)\ln(D_w/D_o)^{n/2}$, where at metal electrodes n is equal to 2 for convective systems and equal to 1 for linear diffusion

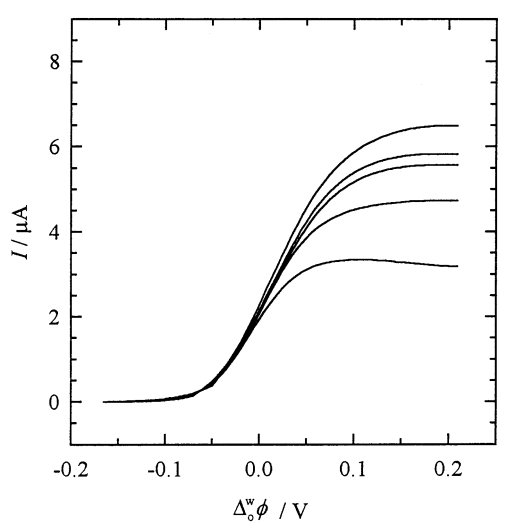

Fig. 9. Experimental linear potential sweeps of TEA^+ transfer at the channel flow water | immobilised *o*-NPOE interface with varying flow rate. Sweep rate 2 mV s^{-1}. Flow rates 121, 312, 511, 711, and 906 $cm^3\ h^{-1}$.

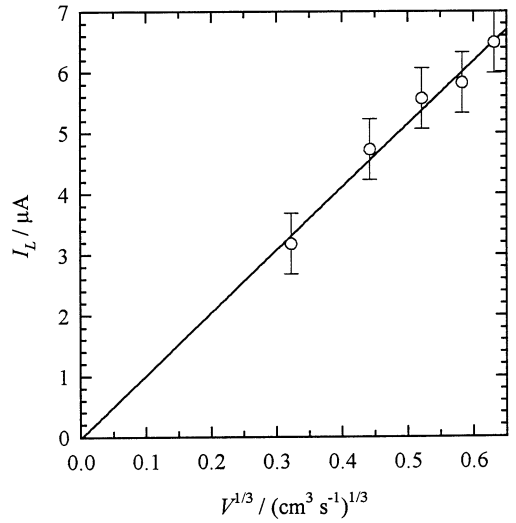

Fig. 10. The limiting current vs. the cubic root of the volume flow rate.

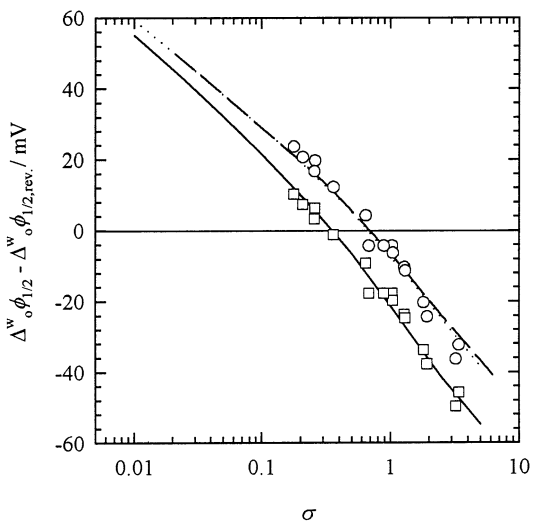

Fig. 11. The difference between the half-wave potential at channel flow and the reversible half-wave potential vs. the dimensionless sweep rate. The full line corresponds to the Singh and Dutt approximation. The other lines have been obtained from the two-dimensional simulations with flow rate of 100 cm^3 h^{-1} (dashed line) and 900 cm^3 h^{-1} (dotted line). The circles and squares are experimental points with $\Delta^w_o\phi^{0'}_{rev} = 8$ and -5 mV, respectively.

only. It can be shown that for this mixed convective/linear diffusion system, $n = 1$. At metal electrodes, $\lim_{\sigma \to 0} \Delta^w_o\phi_{1/2} = \Delta^w_o\phi_{1/2,rev}$ in a CFC. However, in a liquid | liquid CFC, due to the asymmetry in the diffusion regimes, $\Delta^w_o\phi_{1/2}$ does not tend to $\Delta^w_o\phi_{1/2,rev}$ as $\sigma \to 0$. This highlights an important point: the voltammetric response does not tend to a steady state value as the sweep rate is decreased. Instead, $\Delta^w_o\phi_{1/2}$ changes steadily. As the shape of the voltammogram is a function of the dimensionless sweep rate only, so is the difference between $\Delta^w_o\phi_{1/2}$ and $\Delta^w_o\phi_{1/2,rev}$, which is characteristic of the system used. This holds exactly under the Singh and Dutt approximation. The corresponding curves obtained from the two-dimensional simulations are also shown in Fig. 11. The flow rate was fixed at 100 cm^3 h^{-1} (dashed line) or 900 cm^3 h^{-1} (dotted line) and the sweep rate v was varied in order to scan the dimensionless sweep rate σ. These lines are indistinguishable from each other under the conditions usually employed in experiments. Thus, it can be concluded that the shape of the voltammogram is a function of the dimensionless sweep rate only and that the Singh and Dutt approximation is surprisingly accurate also in a CFC utilising a liquid | liquid interface. The points in Fig. 11 are experimental values obtained by changing both the flow rate (between 100 and 900 cm^3 h^{-1}) and the sweep rate (between 1 and 25 mV s^{-1}). The only difference between the two sets (circles and squares) is the value used for $\Delta^w_o\phi_{1/2,rev}$. For the best fit to the Singh and Dutt approximation, $\Delta^w_o\phi_{1/2,rev} = 8$ mV and to a two-dimensional solution, $\Delta^w_o\phi_{1/2,rev} = -5$ mV.

5. Conclusions

This paper demonstrates that it is possible to study ion transfer reactions using a channel flow arrangement at an immobilised ITIES. The theoretical description of the ion transfer has been carried out in terms of average concentration values, which reduces the mathematical problem to one dimension. The validity of this simplification has been tested by simulations of the full, two-dimensional convective diffusion equation. The correspondence between the two approaches has been found to be surprisingly good. Cyclic voltammograms have been simulated for the case of transferring ion initially present in the aqueous phase. The absence of steady state due to the linear diffusion in the organic phase has been observed to be responsible for a shift of the half-wave potential with the dimensionless sweep rate. Cyclic and linear sweep voltammograms have been measured for TEA^+ ion transfer from the aqueous to the organic phase at different flow and sweep rates. As expected, the shape of the cyclic voltammogram is asymmetric thus providing a clear diagnostic criterion for the direction of ion transfer. The experimental half-wave potential was in good correspondence with the theoretical predictions.

Acknowledgements

Financial support from the European Union under project No. ERB-FMRX-CT96-0078 (ODRELLI TMR network) is greatly acknowledged.

Appendix A. Two-dimensional simulations

The discretisation of the transport Eqs. (1a) and (1b) is done in terms of the dimensionless variables

$$C_\alpha = c_\alpha / c_w^b \tag{A1}$$

$$X = x/\Delta x \tag{A2}$$

$$Y_\alpha = y/\Delta y_\alpha \tag{A3}$$

$$T = t/\Delta t \tag{A4}$$

where α denotes either the organic (o) or the aqueous (w) phase. Eqs. (1a) and (1b) then become

$$\frac{\partial C_\alpha}{\partial T} = \lambda_\alpha \frac{\partial^2 C_\alpha}{\partial X^2} + \mu_\alpha \frac{\partial^2 C_\alpha}{\partial Y_\alpha^2} - \beta_\alpha \frac{\partial C_\alpha}{\partial X} \tag{A5}$$

where $\lambda_\alpha = D_\alpha \Delta t/\Delta x^2$, $\mu_\alpha = D_\alpha \Delta t/\Delta y_\alpha^2$, $H = h/\Delta y_w$, $\beta_o = 0$ and

$$\beta_w = -\frac{3V_f \Delta t\, \Delta y_w^2}{4h^3\, w\, \Delta x}\, Y(2H + Y) \tag{A6}$$

The method to solve numerically the problem posed by Eq. (A5) under the boundary conditions shown in Fig. 2 needs to be chosen next. The so-called backward implicit method is very effective for solving transient channel flow problems, but the inclusion of axial diffusion renders it inapplicable [26,27]. The main alternatives are then the explicit method that was used to solve the one-dimensional problem, the so-called hopscotch and alternating direction implicit (ADI) methods, and the strongly implicit procedure (SIP). The standard explicit method is very inefficient with two-dimensional problems [28]. Comparison between the last three has been done by Compton et al. [27], and they found that for transient problems with axial diffusion, ADI was the most effective. In every time step, the ADI algorithm is implicit along one coordinate, with the values for the other coordinate are supplied explicitly from the previous time step. The implicit direction is alternated between successive time steps. For more details, see Refs. [27–29]. The finite difference form of Eq. (A5) for odd time steps (x-direction implicit) is

$$\begin{aligned} &C_\alpha(X, Y, T+1) - C_\alpha(X, Y, T) \\ &\quad = \lambda_\alpha[C_\alpha(X+1, Y, T+1) - 2C_\alpha(X, Y, T+1) \\ &\qquad + C_\alpha(X-1, Y, T+1)] \\ &\qquad + \mu_\alpha[C_\alpha(X, Y+1, T) - 2C_\alpha(X, Y, T) \\ &\qquad + C_\alpha(X, Y-1, T)] - (\beta_\alpha/2)[C_\alpha(X+1, Y, T+1) \\ &\qquad - C_\alpha(X-1, Y, T+1)] \end{aligned} \tag{A7}$$

where the central difference has been used for the convection term. On the even time steps, the finite difference equation is

$$\begin{aligned} &C_\alpha(X, Y, T+1) - C_\alpha(X, Y, T) \\ &\quad = \lambda_\alpha[C_\alpha(X+1, Y, T) - 2C_\alpha(X, Y, T) \\ &\qquad + C_\alpha(X-1, Y, T)] \\ &\qquad + \mu_\alpha[C_\alpha(X, Y+1, T+1) - 2C_\alpha(X, Y, T+1) \\ &\qquad + C_\alpha(X, Y-1, T+1)] \\ &\qquad - (\beta_\alpha/2)[C_\alpha(X+1, Y, T) - C_\alpha(X-1, Y, T)] \end{aligned} \tag{A8}$$

These finite difference equations can be expressed in matrix notation with a tridiagonal coefficient matrix. This permits the use of the Thomas algorithm to solve the resulting set of equations [30,31]. On the even time steps, the boundary conditions at the ITIES are implicitly included in the set of equations. The current is calculated from the concentration values by using a discrete version of Eq. (5) with a five-point approximation of the concentration gradient [28]

$$\begin{aligned} I = \frac{z F D_w w_\sigma c_w^b \Delta x}{12\Delta y_w} \sum_{X=1}^{X_{max}} [&-25C_w(X, 0, T) \\ &+ 48C_w(X, 1, T) - 36C_w(X, 2, T) + 16C_w(X, 3, T) \\ &- 3C(X, 4, T)] \end{aligned} \tag{A9}$$

where X_{max} is the number of grid points over the interface. The number of grid points was adjusted to achieve convergence of current within 1%. Typical values for the number of grid points are shown in Fig. 2. In Fig. 4, however, more grid points were placed both up and downstream of the interface in order to show the concentration profile more fully, i.e. for the sake of clarity of presentation. This did not effect the value of the calculated current. The length of the time step in the range 0.01–0.1 s gave indistinguishable results, at least on the time scale of these simulations (ADI has been reported to oscillate on short time scales when too long a time step is used [27]).

Appendix B. One-dimensional simulations

The one-dimensional diffusion equations ($\alpha = o, w$)

$$\frac{\partial \overline{C_\alpha}}{\partial T} = \mu_\alpha \frac{\partial^2 \overline{C_\alpha}}{\partial Y_\alpha^2} - \gamma_\alpha(\overline{C_\alpha} - 1) \tag{A10}$$

have been solved numerically under the Lévêque approximation

$$\gamma_w = -\frac{3V_f \Delta y_\alpha \Delta t}{2h^2\, w\, l_\sigma}\, Y \tag{A11}$$

by using the explicit finite difference scheme

$$\begin{aligned} &\overline{C_\alpha}(Y, T+1) - \overline{C_\alpha}(Y, T) \\ &\quad = \mu_\alpha[\overline{C_\alpha}(Y+1, T) - 2\overline{C_\alpha}(Y, T) + \overline{C_\alpha}(Y-1, T)] \\ &\qquad - \gamma_\alpha[\overline{C_\alpha}(Y, T) - 1] \end{aligned} \tag{A12}$$

where $\mu_\alpha = D_\alpha \Delta t/\Delta y_\alpha^2$ and $\gamma_o = 0$. Stability of the algorithm requires that $\mu_\alpha \leq 0.5$, and the calculation was performed with $\mu_\alpha = 0.4$. The current was calculated by using a five-point approximation similar to Eq. (A9) and the number of time steps was adjusted to achieve convergence of the current within 1%.

References

[1] A.A. Stewart, G. Taylor, H.H. Girault, J. McAleer, J. Electroanal. Chem. 296 (1990) 491.
[2] J.A. Campbell, H.H. Girault, J. Electroanal. Chem. 266 (1989) 465.
[3] K. Maeda, S. Kihara, M. Suzuki, M. Matsui, J. Electroanal. Chem. 295 (1990) 183.
[4] B. Hundhammer, S. Wilke, J. Electroanal. Chem. 266 (1989) 133.
[5] V. Mareček, M.P. Colombini, H. Jänchenová, P. Papoff, J. Electroanal. Chem. 217 (1987) 213.
[6] E. Wang, H. Ji, Electroanalysis 1 (1989) 75.
[7] J.A. Manzanares, R. Lahtinen, B. Quinn, K. Kontturi, D.J. Schiffrin, Electrochim. Acta 44 (1998) 59.
[8] R.G. Compton, P.R. Unwin, J. Electroanal. Chem. 205 (1986) 1.
[9] K.Y. Tam, C.W. Lee, R.G. Compton, Electroanalysis 9 (1997) 219.
[10] R.G. Compton, B.A. Coles, J. Electroanal. Chem. 144 (1983) 87.
[11] C.M.A. Brett, A.M.C.F. Oliveira Brett, in: C.H. Bamford, R.G. Compton (Eds.), Comprehensive Chemical Kinetics, vol. 26, Elsevier, Amsterdam, 1986, Ch. 5.
[12] V. García, J. Zúñiga, J.A. Manzanares, poster presentation at the Euroconference, Majvik, Kirkkonummi, Finland, 28 August–3 September, 1999.
[13] V.G. Levich, Physicochemical Hydrodynamics, Prentice-Hall, Englewood Cliffs, NJ, 1962, p. 112.
[14] R.G. Compton, R.A.W. Dryfe, R.G. Wellington, J. Hirst, J. Electroanal. Chem. 383 (1995) 13.
[15] T. Singh, J. Dutt, J. Electroanal. Chem. 190 (1985) 65.
[16] R.G. Compton, M.B.G. Pilkington, G.M. Stearn, P.R. Unwin, J. Electroanal. Chem. 238 (1987) 43.
[17] M.A. Lévêque, Ann. Mines Mem. Ser. 12 13 (1928) 201.
[18] M. Abramowitz, I.A. Stegun, Handbook of Mathematical Functions, Dover, New York, 1965, p. 446.
[19] R.G. Compton, P.R. Unwin, J. Electroanal. Chem. 206 (1986) 57.
[20] V. Cunnane, D.J. Schiffrin, C. Beltran, G. Geblewicz, T. Solomon, J. Electroanal. Chem. 247 (1988) 203.
[21] H.J. Lee, P.D. Beattie, B.J. Seddon, M.D. Osborne, H.H. Girault, J. Electroanal. Chem. 440 (1997) 73.
[22] R.G. Compton, P.R. Unwin, J. Electroanal. Chem. 264 (1989) 27.
[23] R.G. Compton, B.A. Coles, J. Electroanal. Chem. 127 (1981) 37.
[24] T. Ohkouchi, T. Kakutani, T. Osakai, M. Senda, Anal. Sci. 7 (1991) 371.
[25] A.J. Bard, L.R. Faulkner, Electrochemical Methods, Wiley, New York, 1980, p. 160.
[26] A.C. Fisher, R.G. Compton, J. Appl. Electrochem. 22 (1992) 38.
[27] J.A. Alden, R.G. Compton, J. Electroanal. Chem. 402 (1996) 1.
[28] D. Britz, Digital Simulation in Electrochemistry, Springer-Verlag, Berlin, 1988.
[29] J. Heinze, M. Störzbach, Ber. Bunsenges. Phys. Chem. 90 (1986) 1043.
[30] R.G. Compton, M.B.G. Pikington, G.M. Stearn, J. Chem. Soc. Trans. I 84 (1988) 2155.
[31] W.H. Press, B.P. Flannery, S.A. Teukolsky, W.T. Vetterling, Numerical Recipes in C, Cambridge University Press, Cambridge, 1988.